

APR 1 1975

Branch Library

NASA CONTRACTOR
REPORT

NASA CR-129023

FEASIBILITY OF REMOTE EVAPORATION AND
PRECIPITATION ESTIMATES

By Willz Z. Sadeh
Colorado State University
Fort Collins, Colorado 80521

April 1974

Prepared for

NASA-GEORGE C. MARSHALL SPACE FLIGHT CENTER
Marshall Space Flight Center, Alabama 35812

TECHNICAL REPORT STANDARD TITLE PAGE

1. REPORT NO. NASA CR-129023		2. GOVERNMENT ACCESSION NO.		3. RECIPIENT'S CATALOG NO.	
4. TITLE AND SUBTITLE FEASIBILITY OF REMOTE EVAPORATION AND PRECIPITATION ESTIMATES				5. REPORT DATE April 1974	
				6. PERFORMING ORGANIZATION CODE	
7. AUTHOR(S) Willz Z. Sadeh				8. PERFORMING ORGANIZATION REPORT #	
9. PERFORMING ORGANIZATION NAME AND ADDRESS Colorado State University Fort Collins, Colorado 80521				10. WORK UNIT NO.	
				11. CONTRACT OR GRANT NO. NAS 8-28590	
				13. TYPE OF REPORT & PERIOD COVERED Contractor Topical	
12. SPONSORING AGENCY NAME AND ADDRESS National Aeronautics and Space Administration Washington, D.C. 25046				14. SPONSORING AGENCY CODE	
15. SUPPLEMENTARY NOTES Prepared under the technical monitorship of the Aerospace Environment Division, Aero-Astroynamics Laboratory, NASA-Marshall Space Flight Center.					
16. ABSTRACT Air pollution levels depend strongly upon the spatial and time variations of various pollutant concentrations. In the vicinity of pollution sources locally high concentrations and significant variation in time of pollutants occur. Surveillance of pollutant concentrations and dispersion requires adequate monitoring over large relevant areas at fixed time intervals. Particularly, strong and stable temperature inversions can cause circulation conditions where vertical mixing of pollutants is prohibited. Remote sensing by means of stereo images obtained from flown cameras and scanners provides the potential to monitor the dynamics of pollutant mixing over large areas. Moreover, stereo technology may permit monitoring of pollutant concentration and mixing with sufficient detail to ascertain the structure of a polluted air mass. Consequently, stereo remote systems can be employed to supply data to set forth adequate regional standards on air quality. Furthermore, methods to detect unpredicted and significant variations in pollution levels can be developed. A method of remote sensing using stereo images is described. Preliminary results concerning the planar extent of a plume based on comparison with ground measurements by an alternate method, e.g., remote hot-wire anemometer technique, are supporting the feasibility of using stereo remote sensing systems. However, to fully check out its feasibility it is imperative to estimate the height of a polluted air mass. This estimation is currently being carried out.					
17. KEY WORDS Air Pollution Remote Sensing Plume Wake			18. DISTRIBUTION STATEMENT Unclassified-unlimited  Ludie G. Richard Act. Dir., Aero-Astroynamics Laboratory		
19. SECURITY CLASSIF. (of this report) Unclassified		20. SECURITY CLASSIF. (of this page) Unclassified		21. NO. OF PAGES 30	
				22. PRICE Domestic \$3.25 Foreign \$5.75	



U18401 0073932

FOREWORD

This report is one of several to be published from research conducted under NASA Contract No. NAS8-28590, entitled, "Feasibility of Remote Evaporation and Precipitation Estimates." A number of approaches have been and continue to be followed in the conduct of the research. The results presented in this report represent only a portion of the total research effort. Other reports will be published as the research progresses.

The author extends sincere gratitude to Mr. Robert Turner of the Aerospace Environment Division, NASA-Marshall Space Flight Center, under whose guidance this research was done. His encouragement and interest were essential to the undertaking and completion of this report. Sincere appreciation is expressed to the personnel of the Aerospace Environment Division for their review of the report and their helpful suggestions.

TABLE OF CONTENTS

	<u>Page</u>
Introduction.....	1
Analysis of Stereoscopic Images.....	4
Experimental Results.....	10
Concluding Remarks.....	16
References.....	17

LIST OF FIGURES

<u>Figure No.</u>	<u>Title</u>	<u>Page</u>
1a.....	Stereoscopic Imagery.....	20
1b.....	Determination of Pollution Target Height by Stereoscopic Comparison and Correlation Techniques.....	20
2	Cancellation of Unrelated Signals by the Product Integration Method.....	21
3	View of the Wild RC8 Camera System.....	22
4	Visualization of Smoke Plume Circulation Under Unstable Conditions.....	23
5	Reproduction of Colored Stereo-Image Triplets of Smoke Circulation Taken from an Altitude of 2000 Ft.....	24
6	Planar Extent of Visible Smoke Plume and Its Corresponding Invisible Plume.....	25

INTRODUCTION

Broadly, changes in the constituents of air either by addition to and/or subtraction from them which affect the physical and/or chemical properties of the air, and subsequently cause detectable deterioration of air quality may be defined as air pollution. Pollutants include any natural and artificial (man-made) airborne contaminants capable of altering air properties. Air pollutants can occur in form of gases, liquid droplets and solid particles, either separately or in mixtures. Gaseous pollutants constitute approximately 90% of the total mass entering the atmosphere while the other 10% are made up of particulates and liquid aerosols [1]. Pollutants emitted directly from identifiable sources are classified as primary pollutants. On the other hand, pollutants produced by interactions among primary pollutants or by reactions with atmospheric constituents are categorized as secondary pollutants [2]. These pollutants can be hazardous to both plant and animal life. By and large, the most harmful air pollution is due to the production of acid droplets through the interaction of sulfuric and nitric oxides with humid air. These oxides evolve primarily from combustion of fossil fuel and refuse.

A complete description of polluted air masses is quite difficult since generally the polluting entities do not retain their exact identities after entering the atmosphere. Pollutants undergo thermal and photochemical reactions with continuous spatial and time variations. In the vicinity of polluting sources locally high concentrations and significant changes in time may occur. Subsequent dispersion depends strongly upon the prevailing winds, atmospheric stability and topographic features. Levels of pollutants are determined in terms

of concentration density, i.e., concentration per unit volume. Similar health hazards can arise from a short time exposure of a few minutes to locally high concentrations or of long time exposures of hours and even days to low concentrations.

Detection of pollution through direct sampling is rather complex since a great number of sampling stations distributed over large areas are needed. In the United States there are over 7,000 sampling stations [1]. Most of these stations, however, are located in metropolitan and industrial areas, i.e., in area sources and in the vicinity of major point sources such as high smoke stacks. To monitor the spatial and time variations of pollutants to obtain contour maps of trace constituents, surveys within relatively large distances downstream of the sources are required. For instance, aerial photographs of power plants reveal that the most dangerous surface pollution concentrations occur within 5 to 10 km downwind of the plants in the case of a limited mixing plume [3]. Even surface concentrations at distances beyond 30 km from the source were detected for fanning and inversion breakup plumes [3]. Surveys of plume rise and dispersion over such large areas using sampling stations are costly and inherently difficult due to the continuous changing meteorological conditions. Moreover, the use of sampling stations to monitor line sources such as highways and runways (mobile sources), and unpredictable downwind precipitation areas is practically precluded due to the extreme range of area involved and the wide changes in concentration. In many cases, furthermore, the setup of sampling stations is prevented by local safety regulations, e.g., erection of tall meteorological towers in vicinity of airports.

Pollutants are deposited into the atmospheric boundary layer where they are conveyed either as active or passive scalars by advection and turbulent diffusion. In the atmosphere the turbulent diffusion depends

on both shear flow and vertical temperature distribution. The buoyancy forces, which are determined by the temperature variation, play a prime role in the dynamics of air motion. When stable conditions prevail, i.e., subadiabatic temperature lapse rates, the turbulent diffusion of contaminants is retarded by buoyancy forces. The extreme case of stable conditions is represented by temperature inversions. Strong and stable inversion layers yield extreme circulation conditions where vertical turbulent mixing of pollutants is effectively prohibited by the temperature lid. Dangerous inversion which can persist for several days usually develop within high pressure ranges. Over urban areas temperature inversions are commonly found beyond a certain mixing depth [4, 5]. Generally, the urban inversions arise in the form of a dome-shaped envelope due to the uneven heat distribution. Furthermore, on clear mornings at sunrise and often on evenings at twilight with light winds or calm conditions near the surface, a base inversion layer occurs. This layer may extend from the ground up to heights of 150 to 750 m depending upon the local topographic configuration [6]. Simultaneously, a second inversion layer may exist at higher altitudes [6]. Inside an inversion layer the highest surface concentrations occur within 5 to 10 km downwind of the sources and can persist for prolonged time depending upon the type and lifetime of the inversion [3].

Air pollution surveys are strongly dependent on detailed knowledge of prevailing turbulent winds and atmospheric stability conditions within relevant large areas. Remote-sensing technology possesses the potential to monitor both meteorological parameters and needed data on the dynamics of mixing of pollutants in sufficient detail and within substantial large areas. The orbital stereo photographs taken during the Gemini missions clearly substantiate the use of stereo techniques

to survey contaminated air masses over exceedingly large areas [7]. Furthermore, advance detection of unexpected pollution is feasible. As a result, adequate regional air quality standards and control regulations can be set forth. However, to determine chemical composition of pollutants, size and distribution of particulates and health endangerment levels, direct sampling is needed. Remote sensing by means of stereoscopic observations is capable of yielding a host of information which can augment manifold the knowledge on the dynamics of mixing of pollutants and surface concentrations.

ANALYSIS OF STEREOSCOPIC IMAGES

Stereoscopic viewing of targets essentially reduces to stereo comparison of a pair of images with some overlapping areas. Such two successive photographs can be taken by a precision aerial camera along the flight path of an aircraft. Two pictures taken in succession and the corresponding overlapping areas indicated by shaded regions I and II are shown in Fig. 1(a). Next, two arbitrary objects are selected within the area of overlap. They are denoted by 1 and 2 in the first photograph while their conjugate images in the second picture are designated by 1' and 2', respectively. These objects can be a sharp ground feature and a tenuous but visible polluted air mass as portrayed in Fig. 1(b). Under the assumption of a fixed (stationary) pollution target, the height and three-dimensional extent of the plume can be determined by stereoscopic comparison of the two images [8]. Thus, the time lapse between two successive exposures must be short enough such that the distance traveled by the pollution target can be disregarded. The human matching of the stereo images is carried out using a stereocomparator. Subsequent

attempts to align the pollution target will lead to a mismatch for the ground object. This misalignment is caused by the fact that the two targets are situated at different heights. The distance difference, i.e., the parallactic distance, can be estimated from the mismatch of the ground reference object as illustrated in Fig. 1(b). Then, the height of the pollution target is computed by triangulation utilizing the parallactic distance and the difference in the view angles from the two images for the pollution target (the parallactic angles). This method can also be used to estimate the features of an inversion layer. When the motion of the polluted mass is not negligible, a third stereo image is needed. Then, two independent parallactic distances are obtained. Similar triangulations yield both plume altitude and its horizontal velocity.

Results using this stereo analysis to deduce the three-dimensional extent of visible plumes are reported in Ref. 9. The three-dimensional extent of plumes were estimated using vertical and oblique stereo image pairs with 60% overlap taken at altitudes of 10,000 and 15,000 ft, respectively. The accuracy of this method decreases drastically with distance from the source. At 3 miles downwind of the polluting source, the error in approximating the plume height is ± 100 ft [9]. Beyond this range, evaluation of plume height becomes uncertain. Human photogrammetric stereo comparison is limited even under optimum conditions. For barely visible and invisible plumes such as oxide gases, human stereo interpretation is completely impractical. With increased use of precipitators in high smoke stacks, the visibility problem becomes more compound.

The stereoscopic analysis of images can be highly improved and refined when adequate digital cross-correlation techniques are utilized. Initially, these techniques were developed and employed for remote measurement of sound sources, heat radiation, wind, and turbulence using passive optical crossed beams [10, 11, 12]. The crossed-beam correlation method was further applied to active sensors. A review of the applications of electromagnetic correlation techniques can be found in Ref. 13. Basically, this method combines remote measurements with adequate data processing and statistical analysis.

To carry out digital correlation of a stereoscopic image pair, conversion of each picture into discrete scan lines is necessary [14]. These lines, which are depicted in Fig. 1(a), can be obtained by scanning stereo photographs with a microdensitometer [9, 15]. Essentially, the discrete scan lines constitute the scan history of the image in the form of a digitized record of the radiation power within a certain field of view. The scan history consists of a sufficient number of adjacent scan lines which supply an image of the target area in terms of a strip map. It is, further, important to note that scan histories within wavelength ranges where photographic emulsions are not available can be supplied by utilizing electromechanical stereoscopic scanners.

The scan history can be expressed in terms of a signal

$$x(t) = x(m,n) , \quad (1)$$

where m designates the scan line number relative to the position of a ground reference object whose scan line is $m = 0$. The sample point number along a particular scan line is denoted by n . It is determined with respect to the sample point $n = 0$ that intersects the ground reference feature.

The stereo analysis is performed by computing the cross-covariance function of the two overlapping areas I and II. To calculate the cross-covariance, one of the images, e.g., image II, is delayed by k scan lines and ℓ sample points. Then, the sample cross-covariance estimate is

$$C_{xy}(k, \ell) = \frac{1}{4MN} \sum_{-M}^M \sum_{-N}^N x(m, n) y(m+k, n+\ell) , \quad (2)$$

where $x(m, n)$ is the signal from image I, and $y(m+k, n+\ell)$ is the delayed signal from the overlaying area II. The number of resolution elements per strip is denoted by $4MN$. A direct quantitative measure for the matching is provided by the cross-covariance. The best match of the features related to the pollution mass is indicated by the peak value of the cross-covariance. In a similar manner, but independently, the match of the ground reference can be obtained. As a result, the parallax distance is obtained and, then, the plume features (or inversion characteristics) are evaluated by triangulation as portrayed in Fig. 1(b).

The signals from stereo images are random variables of time and, thus, they can be expressed as

$$x(t) = x_1(t) + x_2(t) , \quad (3.1)$$

and

$$y(t) = y_1(t) + y_2(t) , \quad (3.2)$$

where the subscripts 1 and 2 denote the target signal and transmission noise, respectively. Then, the cross-covariance is

$$\begin{aligned} \overline{C_{xy}(\tau)} &= \overline{x_1(t) y_1(t + \tau)} + \overline{x_1(t) y_2(t + \tau)} \\ &+ \overline{x_2(t) y_1(t + \tau)} + \overline{x_2(t) y_2(t + \tau)} , \end{aligned} \quad (4)$$

where the τ designates the time delay, and the overbar denotes time integration over the entire scan history. The first term on the right-hand side of Eq. (4) is the cross-covariance of the common signals. It is important to remark that this product is always positive since both signals are of same sign being generated by the same random process [12]. In other words, both stereo images are affected in a similar way by the polluted air mass target. This is true provided that the motion of the pollution target is disregarded, i.e., a stationary target. The other three products represent cross-covariances of uncorrelated random variables caused by statistically independent random processes. Consequently, they vanish provided that the integration time is long enough. Basically, the cross-covariance is dominated by the product $\overline{x_1 y_1}$. This term increases linearly with integration time. On the other hand, the other three terms produce oscillations with equal likelihood about the average value, i.e., negative and positive oscillations. Their contributions to the time integral increase with the square root of integration time [12]. Adequate averaging methods to cancel the noise by product integration for finite integration time are proposed in Ref. 12.

The mean square error of the cross-covariance estimate due to individual resolution element (or finite integration time) is given by the variance,

$$\text{Var}[C_{xy}(k, \ell)] = \frac{1}{4MN-1} \sum_{m,n} [x(m,n)y(m+k, n+\ell) - \bar{C}_{xy}]^2, \quad (5)$$

since $C_{xy}(k, \ell)$ is an unbiased estimate of the true value of the cross-covariance \bar{C}_{xy} [16]. Moreover, the mean square error decreases with increasing integration time. Next, the confidence to obtain a

meaningful match is expressed by the ratio of the cross-covariance estimate to its root-mean-square (rms) error

$$\alpha_{k,\ell} = \frac{C_{xy}(k,\ell)}{\sqrt{\text{Var}[C_{xy}(k,\ell)]}} , \quad (6)$$

which is the coefficient of confidence.

In practice, additional limitations exist due to the uncontrolled effects of the optical environment. Averaging techniques employing the variations of piecewise mean values to recognize and eliminate these effects were attempted [12]. A sample of the instantaneous product xy of two total signals for two different wavelength ranges from a stereo scanner is shown in Fig. 2. The continuous strongly oscillating curve represents the scan time history. The cumulative average of the instantaneous product

$$C_{xy}(k,\ell,T) = \frac{1}{T} \int_0^T x(k,\ell,t) y(k,\ell,t) dt , \quad (7)$$

is a function of the variable record length (or integration time), $0 < T < 2MN$. With increasing integration time the variations of the cumulative average diminish since the changes in the instantaneous product cancel each other. The negative fluctuations of the instantaneous product represent signal components which are unrelated to the target since the contribution of the common signals from the polluted mass to the instantaneous product is always positive. Moreover, the positive instantaneous products also contain signals which are uncorrelated to the pollution target. These positive products cancel the negative products. The shaded areas in Fig. 2 delineates the power of the irrelevant signals. Their cancellation through the integration process is indicated by the decreasing change in the variations of the cumulative average. Furthermore, with increasing number of instantaneous products

the mutual cancellation of the unrelated signals is enhanced. This process of cancellation by product integration is completed when the cumulative average reaches a constant value [12, 14]. Practically, this value represents the power of the common signals from the pollution target. Consequently, the product integration process permits recovery of very weak signals provided that the target is sufficiently large and homogeneous. The latter condition is needed to allow suppression of the noise [12]. This method can eventually be further utilized for a nonhomogeneous polluted mass by subdividing it into homogeneous domains using unsupervised classification techniques [14]. As a result, even tenuous pollution targets are eventually retrievable using this correlation analysis. Furthermore, this technique can be applied to evaluate the water vapor burden within a column of air.

EXPERIMENTAL RESULTS

To demonstrate the feasibility of stereoscopic remote sensing of polluted air masses and of stereo-correlation analysis of stereoscopic images, an extensive field experimental program is currently being conducted. To start with, it was necessary to ascertain the capability of using stereo images to detect the planar extent of a moving pollution target. Subsequently, it is planned, during the second stage of the program, to assess the three-dimensional features of a moving pollution target utilizing the correlation analysis. The objectives of a systematic field experiment could not be achieved by simply surveying pollutants randomly emitted into the atmosphere. It was imperative to surmount the unpredictable effects of continuous meteorological conditions. Furthermore, it was desired to inject pollutants under controlled circumstances into a known flow environment and unchanged flow conditions over a long enough time period.

For these reasons, it was decided to simulate the environmental conditions using the wake flow produced by a 10 ft diameter fan of variable pitch (Hartzell A120-6). This fan constitutes the core of the Colorado State University Environmental Field Station. The fan, which is driven by an internal combustion engine, could produce continuous varying air speeds up to 20 mph. Within the wake large scale turbulence is produced and, consequently, the environmental conditions are adequately simulated for pollutant injection. To reduce undesirable interferences with the ambient winds, all experiments were conducted under calm conditions or light winds up to 2 mph at the most. Continuous monitoring of the prevailing winds was performed using cup anemometers.

Contaminants in the form of gases, liquid and solid particulates can be released under governed conditions from point sources and/or line sources. The pollutants may be emitted either separately or premixed in any desired ratios. Locations of polluting sources were selected based on velocity distribution and turbulence characteristics within the wake to avoid any perturbations generated by the fan supporting structure. The sources, consequently, were located at least 20 ft downstream of the fan. Moreover, since the sources are mobile they can be located in any configuration and at any position of interest. It is worth pointing out that similar sources can be utilized to generate controlled water vapor plumes within the wake.

The Environmental Field Station is located on a flat surface free of immediate natural or artificial obstructions. At the field station almost daily base temperature inversions occur on clear mornings and

in the evenings at twilight. The station is equipped with an Analog Data Acquisition System. In addition, a Digital Data Acquisition System is available at the site for on-line data reduction and analysis. Fixed ground reference targets needed for the stereo photographs were set up.

To ascertain the practical applications of the stereoscopic remote sensing, corresponding ground measurements are necessary. Furthermore, comparison of the results will lead to development of adequate calibration techniques for the stereo remote sensing. Ground measurements of velocity and turbulence were carried out utilizing a novel three-lead hot-wire anemometer system conceived, designed and built at Colorado State University [17]. Generally, the use and performances of hot-wire anemometers depend on the length of the cables connecting the hot wire (the sensor) to the anemometer's bridge. The length of the connecting leads and, hence, their resistance affects strongly the bridge balance, the noise level and the frequency response of the anemometer. The accepted length of the leads is limited to about 25 ft. Whenever longer cables are utilized adequate compensation is required to allow the bridge balance. However, both the noise level and frequency response are increasing and decreasing, respectively, with the cable's length. The new three-lead system removes the cable's length constraint since connecting leads in excess of 500 ft length can be utilized without need for compensation [17]. In this system the balance of the bridge is not dependent upon the length of the connecting cables. The noise level remains practically unaffected by the lead's length, and the decrease in frequency response is negligible. The new remote system affords innumerable applications of hot-wire anemometry techniques in

atmospheric measurements. Specific hot-wire interpretation methods developed for flow with large fluctuations, such as encountered in the atmosphere, are employed [18].

The aerial stereoscopic photographs were taken employing a Wild RC8 automatic precision mapping camera system with 93° coverage (Wild-Heerbrugg Inst.). The camera is equipped with a 6 in. Universal Aviogon lens cone (f/5.6) with rotary shutter. An antivignetting filter Wild A.V. 2.2 x (Wild-Heerbrugg Inst.) is utilized to provide uniform lighting across the lens and, thus, uniform exposure on the film is obtained. All pictures were taken using Kodak aerocolor negative ester base film. Included in the camera system are a driving mechanism, a control box, a viewfinder telescope, a clock, and an altimeter. A general view of the camera system is shown in Fig. 3. The camera produces 9 x 9 in. photographs with remarkably low distortion and high resolution. The former is smaller than 0.01 mm whereas the latter varies from 50 lines/mm in the center to 25 lines/mm in the corners. This high resolution permits adequate conversion of the picture into discrete scan lines for further digital correlation analysis. The film advance per exposure amounts to 10 in. allowing readings of the incorporated clock and altimeter to be recorded on each photograph. Continuous adjustment of the exposure time from 1/1000 to 1/7000 sec is provided by the driving motor. Four overlap areas of 20, 60, 70 and 80%, respectively, are available. The shortest time interval between exposures, i.e., the time lapse, is roughly 3 to 3.5 sec. A plume conveyed by such a velocity that the distance traveled during the time lapse is small compared with its overall horizontal extent will appear on two successive photographs as being approximately stationary. At this

point, it is important to notice that the plume is "stationary" with respect to stereoscopic photography since it will roughly affect a stereo-image pair in the same manner as a ground reference object. Thus, one can consider the plume as being stereoscopically stationary. Such situations occur particularly within inversion layers, light winds or calm conditions. For aerial operation, the camera system is flown in Colorado State University Aero-Commander 500B research aircraft.

Direct measurement and recording of the space coordinates of any desired image on a stereo-photograph pair is carried out utilizing the Wild STK-1 Stereocomparator/Digitizer/IBM Card Punch (Wild-Heerbrugg Inst.). The coordinates of selected objects can be measured with a precision of $1\mu\text{m}$ (1/25,400 in.). It is important to remark that the evaluation of the vertical coordinates may be arduous due to the haze of the plume. Scanning by means of a microdensitometer, which measures the transmittance of the photographic emulsion, can undoubtedly supply more reliable estimation of the vertical extent of the pollution target. Such a scanning is being planned.

Henceforth, the preliminary results of the first stage of the feasibility investigation are presented. To begin with, intensive, although not exhaustive, visualization studies of circulation of visible plumes generated by colored smoke were conducted. The smoke point sources were located at various positions along the streamwise direction of the wake flow and at several elevations above the ground. Several frames from a movie showing the smoke plume circulation, entrainment and dispersion without and with temperature inversion are given by Fig. 4. The fan is also shown in Fig. 4(a). Relatively large scale vortices were clearly discerned when unstable conditions

(superadiabatic lapse rates) prevailed. The photographs shown in Figs. 4(a) and 4(b) were taken under such conditions. Without temperature inversion, the smoke plume is dispersed quickly at higher altitudes due to the vortices within the wake. However, in the neighborhood of the sources, due to the large scale vortices, deposit of pollutants on the ground can occur as indicated by the smoke circulation observed in Fig. 4(b). Under inversion conditions small scale vortices were prominent as illustrated by the photographs shown in Fig. 4(c). Furthermore, relatively high smoke concentrations persisted for a prolonged time. Knowledge of the scale of vortices is essential for the study of both dispersion and concentration of pollutants, and temperature distribution. Within the earth-atmosphere interface, in particular, the prevailing vortices play a prime role in the surface concentration of pollutants.

Next, numerous overflight surveys of the smoke plume were carried out. Stereoscopic photographs were taken from several altitudes. All photographs were obtained with 60% overlap and with a time lapse of 3 sec. The aerial photogrammetric surveys were conducted either under calm conditions or light winds up to about 1 mph and temperature inversion. A stereo-image triplet of smoke circulation taken from an altitude of 2000 ft is shown in Fig. 5. Analysis of the stereo images by means of a stereocomparator revealed that the maximum measurable windwise extent of the plume was about 70 ft. The shape and extent of the smoke plume in the horizontal plane is depicted in Fig. 6. For a wind speed of 1.5 ft/sec (\approx 1 mph), the smoke plume traveled a distance of 4.5 ft during the time lapse. Since this distance is about 6.4% of its windwise range, one can conceivably assume that, for most practical purposes, the plume

could be considered stereoscopically stationary. The similar extent of the smoke plume obtained by comparison of a series of stereo images taken under same conditions substantiates the foregoing conclusion.

Basically, the smoke plume was produced by injecting smoke into the wake. The smoke was then transported by the flow and practically entrained throughout almost the entire wake. Hence, the wake can be considered as being an invisible plume whose overall spatial extent roughly coincides with that of the visible smoke plume. To corroborate the horizontal extent of the smoke plume deduced from the stereo images, hot-wire anemometer ground measurements of the planar extent of the corresponding invisible plume were performed. These measurements were conducted under same wind and inversion conditions as for the remote stereo survey but not simultaneously. The boundary of the invisible plume, i.e., the wake boundary, was defined as the location where the local streamwise velocity reduces to about 2% of the fan rotor tip velocity [19]. The results of the hot-wire anemometer survey are shown in Fig. 6 together with the horizontal extent of the visible smoke plume. A striking similarity between the extents of the visible and invisible plumes is clearly discerned. Their planar extents coincide within $\pm 10\%$. This consistent general congruence substantiates the feasibility of using stereo images. Note that this agreement was obtained for a relatively small, tenuous plume as clearly indicated by Fig. 5. Thus, stereo images can be used to survey even barely visible and weak plumes. Currently, the evaluation of the three-dimensional features of the plume, i.e., stereoscopic estimation of the height using digital correlation analysis, is underway.

CONCLUDING REMARKS

The feasibility of stereoscopic remote sensing of polluted air masses by means of flown stereo cameras is indicated by the preliminary results presented in this work. The evaluation of the planar extent of a plume based on both stereo images and ground measurements exhibits a reasonable agreement. Even tenuous plumes of relatively limited spatial extent can be monitored using stereo images. In this experiment the windwise extent of the plume was roughly 70 ft.

Analysis of a stereo-image pair can be used to establish the features of a moving polluted air mass provided that the condition of stereoscopic stationarity is satisfied. When the distance traveled by a plume during the time lapse between two successive exposures is small compared with its overall horizontal extent, one can assume that the plume is stereoscopically stationary. This situation usually occurs within temperature inversion layer, under light winds or calm conditions. When the condition of stereoscopic stationarity is not fulfilled, e.g., strong winds, a stereo-image triplet may be necessary. Currently, analysis of such triplets is being attempted.

By and large, standard stereo comparison analysis is limited due to variations in the concentration of pollutants within the plumes, the haze of the plumes, and the continuous changing optical background. Digital stereoscopic analysis based on correlation techniques may possess the potential to overcome these difficulties. An intensive effort to demonstrate the efficacy of digital stereo correlation is planned. It is expected that the completion of the correlation analysis of stereo-image pair and triplet, which is currently in progress, will hopefully provide the needed support for the feasibility of remote stereoscopic survey of polluted air masses. The development of mathematical models for long

term pollution distribution and concentration over large areas depends, to a large extent, on detailed knowledge of both meteorological conditions and polluted air mass features. Stereoscopic techniques eventually can be used efficiently to provide contour maps of pollution including isoconcentration density curves in addition to meteorological parameters.

REFERENCES

1. Morgan, G. B., Ozolins, G. and Tabor, E. C., "Air Pollution Surveillance Systems," *Science*, 170, 3955, 280-296 (1970).
2. Chambers, L. A., "Classification and Extent of Air Pollution Problems," *Air Pollution*, edit., Stern, A. C., Vol. 1, Air Pollution and Its Effects, 1-22, Academic Press, New York 2nd ed. (1968).
3. Carpenter, C. B., Leavitt, J. M., Colbaugh, W. C. and Thomas, F. W., "Principal Plume Dispersion Models TVA Power Plants," 63rd Annual Meeting, Air Pollution Control Association, 14-18 June 1970, St. Louis, Missouri (1970).
4. Hoffert, M. I., "Atmospheric Transport, Dispersion, and Chemical Reactions in Air Pollution: A Review," *AIAA Journal* 10, 4, 377-387 (1972).
5. Davidson, B., "A Summary of the New York Urban Air Pollution Dynamic Research Program," *J. Air Pollution Control Assoc.*, 17, 3, 154-158 (1967).
6. Wanta, R. C., "Meteorology and Air Pollution," *ibid.*, Ref. 2, 187-226.
7. Wobber, F. J., "Orbital Photos Applies to the Environment," *J. Photogrammetric Eng.*, 26, 8, 852-864 (1970).
8. Moffit, F. H., *Photogrammetry*, International Textbook Co., Scranton, Penn., 2nd ed. (1967).
9. Veress, S. A., "Air Pollution Research," *J. Photogrammetric Eng.* 26, 8, 840-848 (1970).
10. Fisher, M. J. and Krause, F. R., "The Crossed-Beam Correlation Technique," *J. Fluid Mech.*, 28, 4, 705-717 (1967).
11. Krause, F. R., Derr, V. E., Abshire, N. L., and Strauch, R. G., "Remote Probing of Wind and Turbulence Through Cross-Correlation of Passive Signals," Proceedings, 6th International Symposium on Remote Sensing of Environment, 13-16 October 1969, Univ. of Michigan, Ann Arbor, Mich., 327-357 (1969).

12. Krause, F. R., Su, M. Y. and Klugman, E. H., "Passive Optical Detection of Meteorological Parameters in Launch Vehicle Environments," J. Applied Optics, 9, 5, 1044-1055 (1970).
13. Krause, R. F., edit., "Research on Electromagnetic Correlation Techniques," NASA TM X-64505, George C. Marshall Space Flight Center, NASA, Huntsville, Alabama (1970).
14. Krause, F. G., Betz, H. T. and Lysobey, D. H., "Pollution Detection by Digital Correlation of Multispectral Stereo-Image Pairs," AIAA Paper No. 71-1106, Joint Conference on Sensing of Environmental Pollutants, 8-10 November 1971, Palo Alto, Calif. (1971).
15. Data Corporation Manual, "Man-Made Micro-Analyzer," Data Corp. Dayton, Ohio (1968).
16. Bendat, J. S. and Piersol, A. G., Random Data: Analysis and Measurement Procedures, Wiley-Interscience, New York (1971).
17. Sadeh, W. Z. and Finn, C. L., "A Method for Remote Use of Hot Wire Anemometer," Review Scient. Instrums., 42, 9, 1376-1377 (1971).
18. Sadeh, W. Z., Maeder, P. F. and Sutera, S. P., "A Hot Wire Method for Low Velocity with Large Fluctuations," Review Scient. Instrums., 41, 9, 1295-1298 (1970).
19. Koper, C. A., Jr., and Sadeh, W. Z., "A Preliminary Study of a Fan Wake," RM CEM70-71CAK-WZS23, Dept. of Civil Eng., Colorado State University, Fort Collins, Colorado (1971).

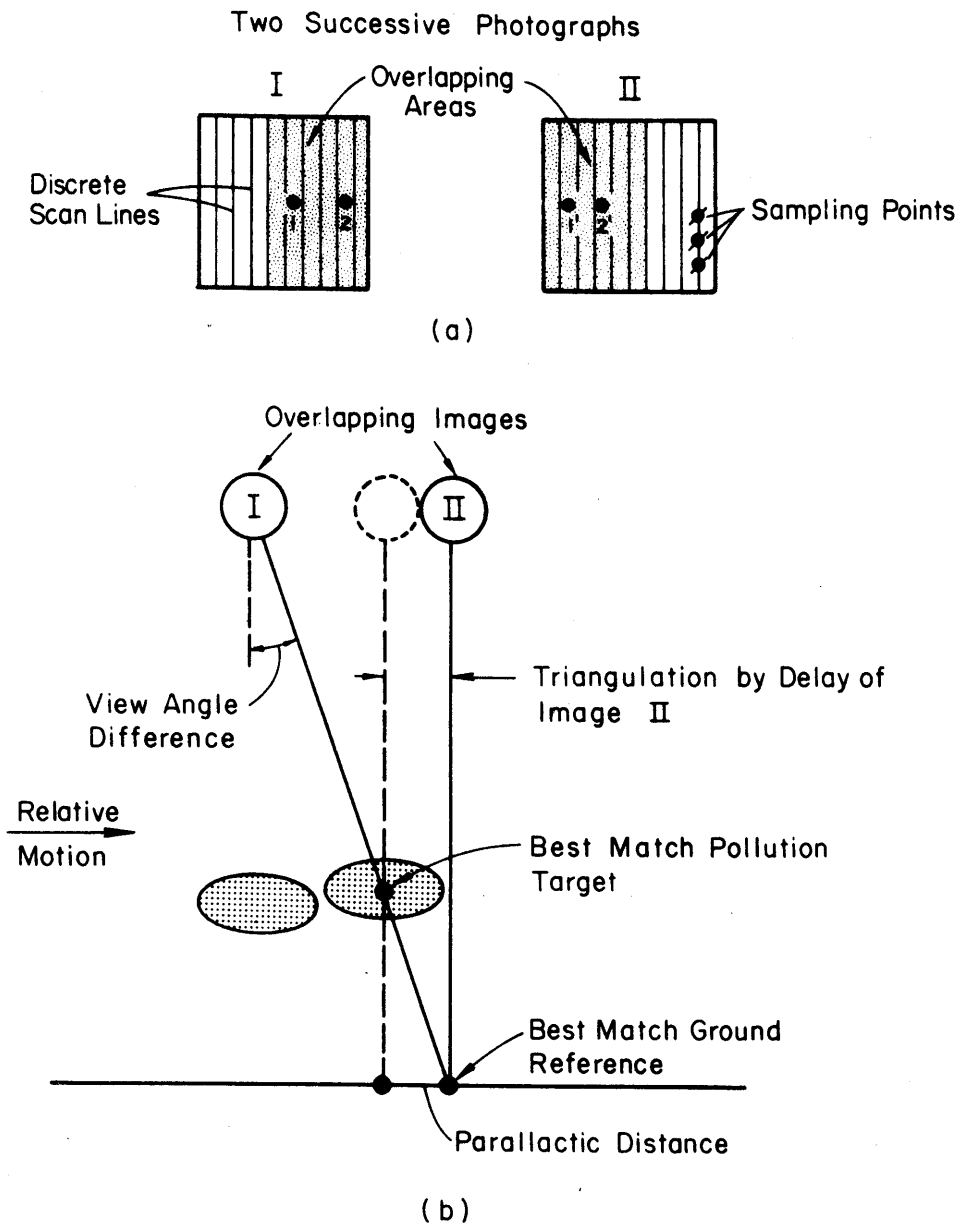


Fig. 1 (a) Stereoscopic imagery. (b) Determination of pollution target height by stereoscopic comparison and correlation techniques.

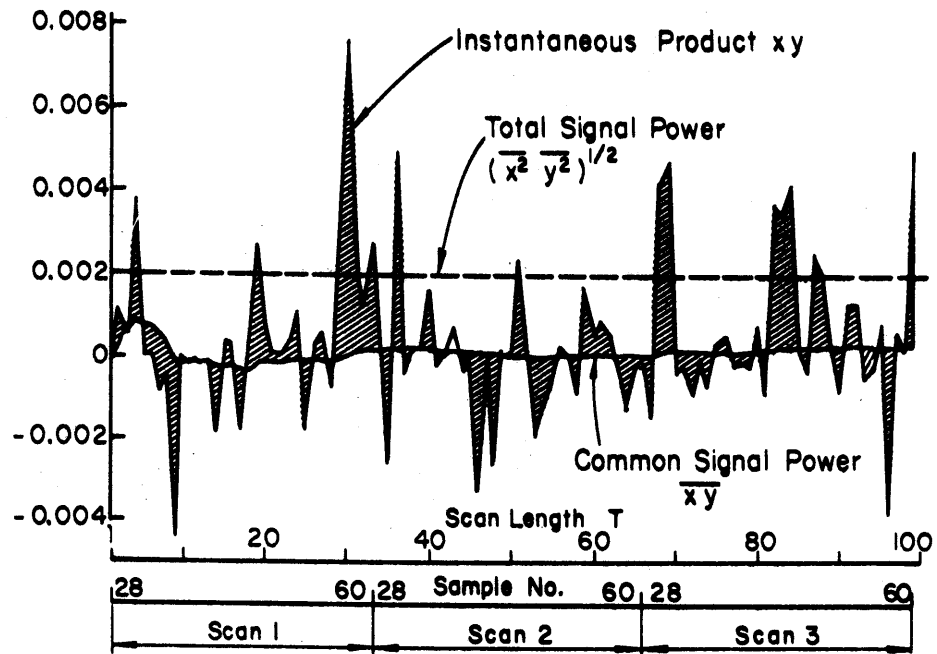


Fig. 2 Cancellation of unrelated signals by the product integration method.

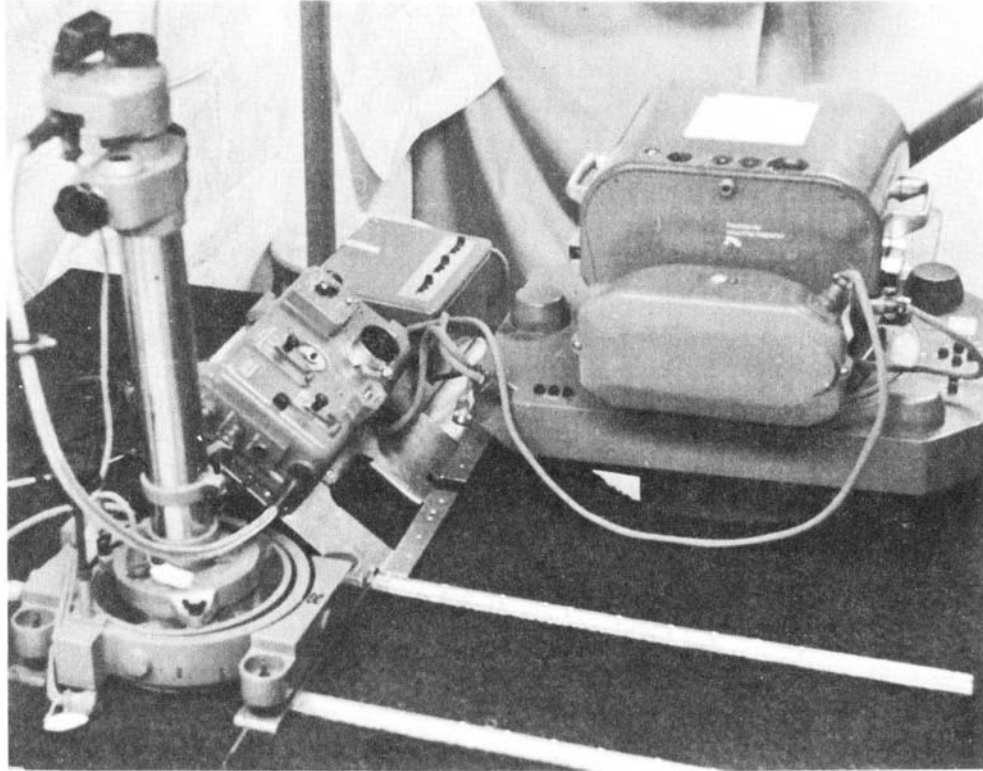
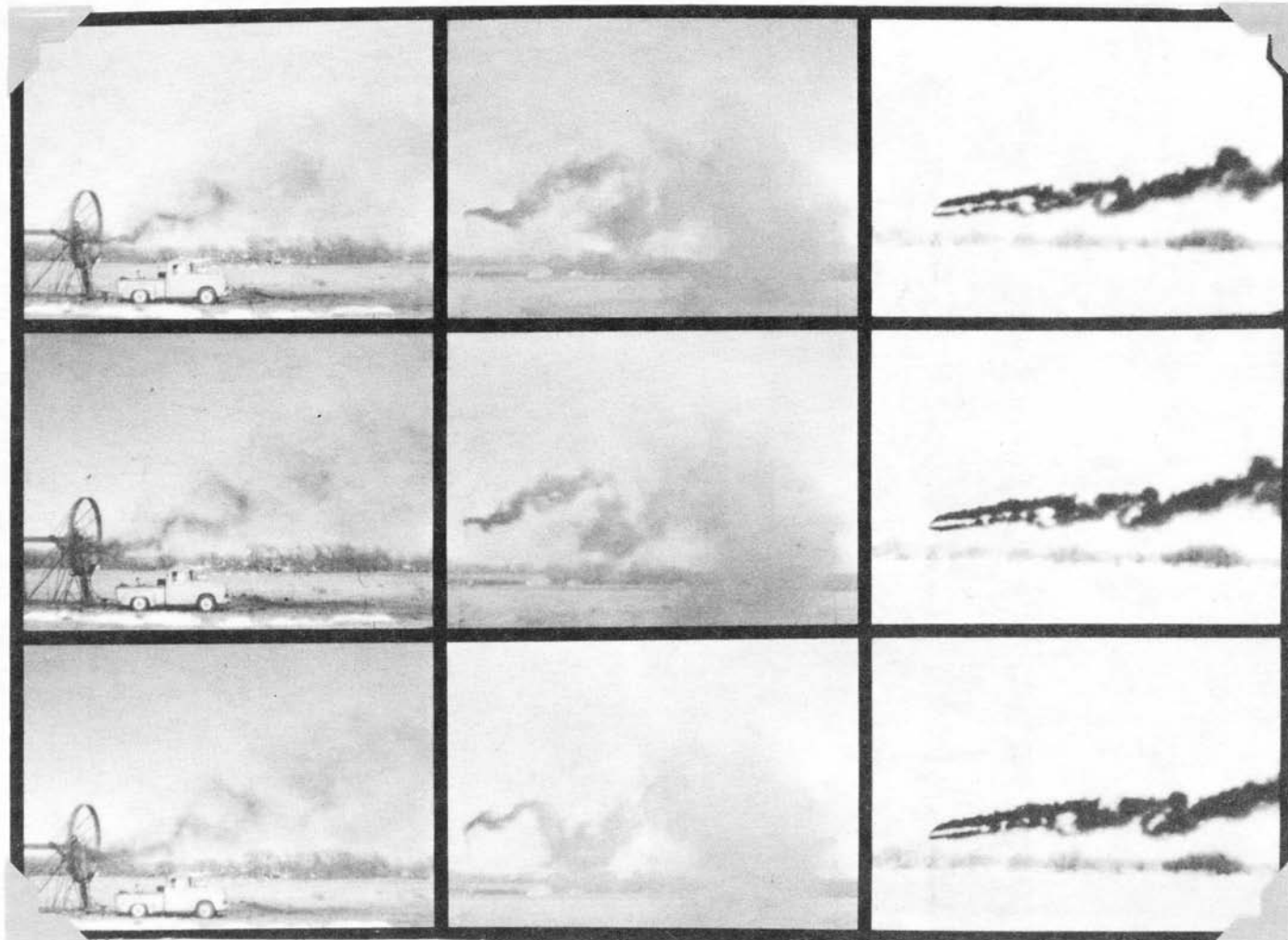


Fig. 3 View of the Wild RC8 camera system.

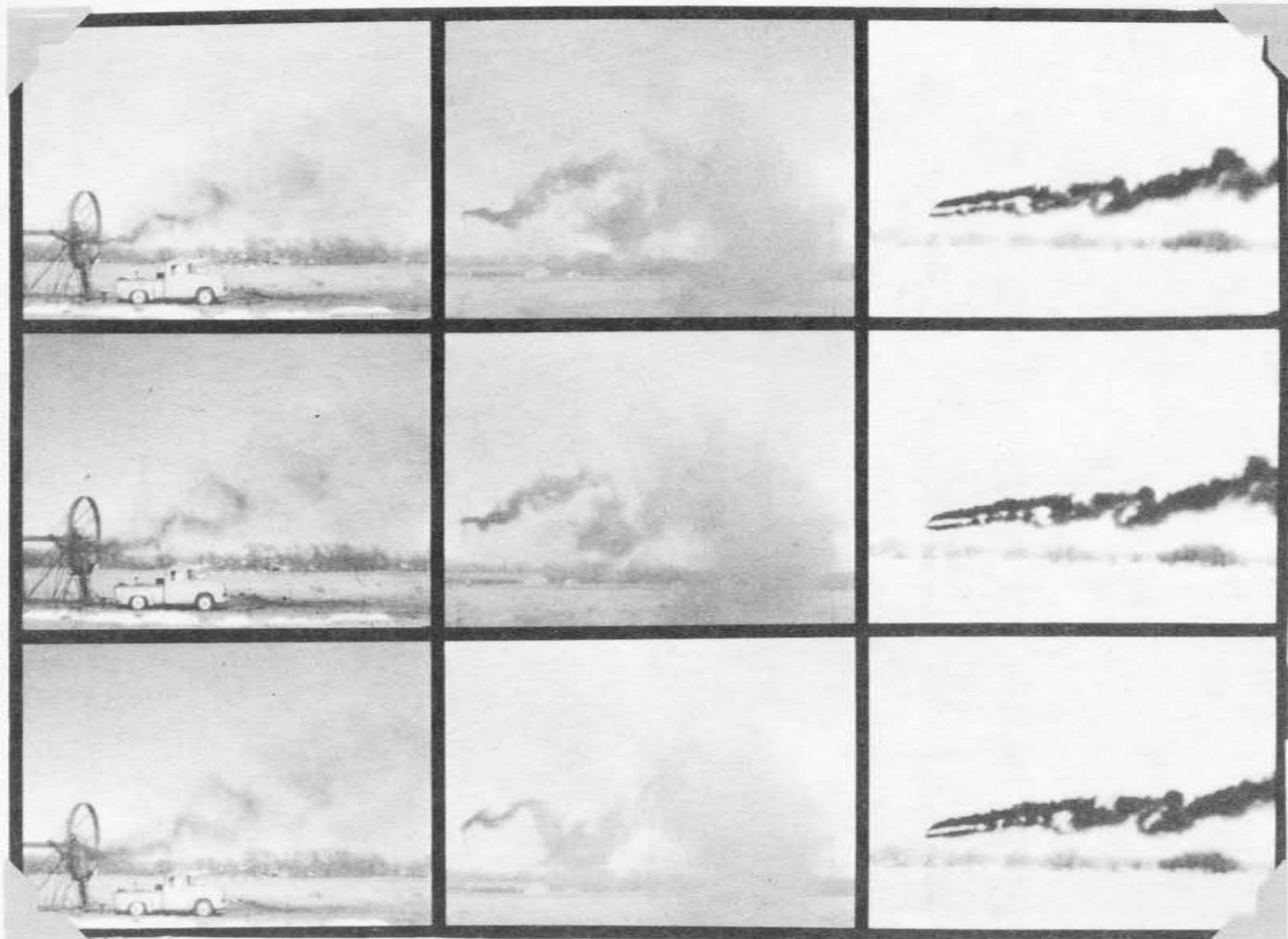


(a)

(b)

(c)

Fig. 4 Visualization of smoke plume circulation under unstable conditions: (a) point source upstream of the fan; and, (b) point source at 40 ft downstream of the fan; and within a temperature inversion layer: (c) point source at 150 ft downstream of the fan.



(a)

(b)

(c)

Fig. 4 Visualization of smoke plume circulation under unstable conditions: (a) point source upstream of the fan; and, (b) point source at 40 ft downstream of the fan; and within a temperature inversion layer: (c) point source at 150 ft downstream of the fan.

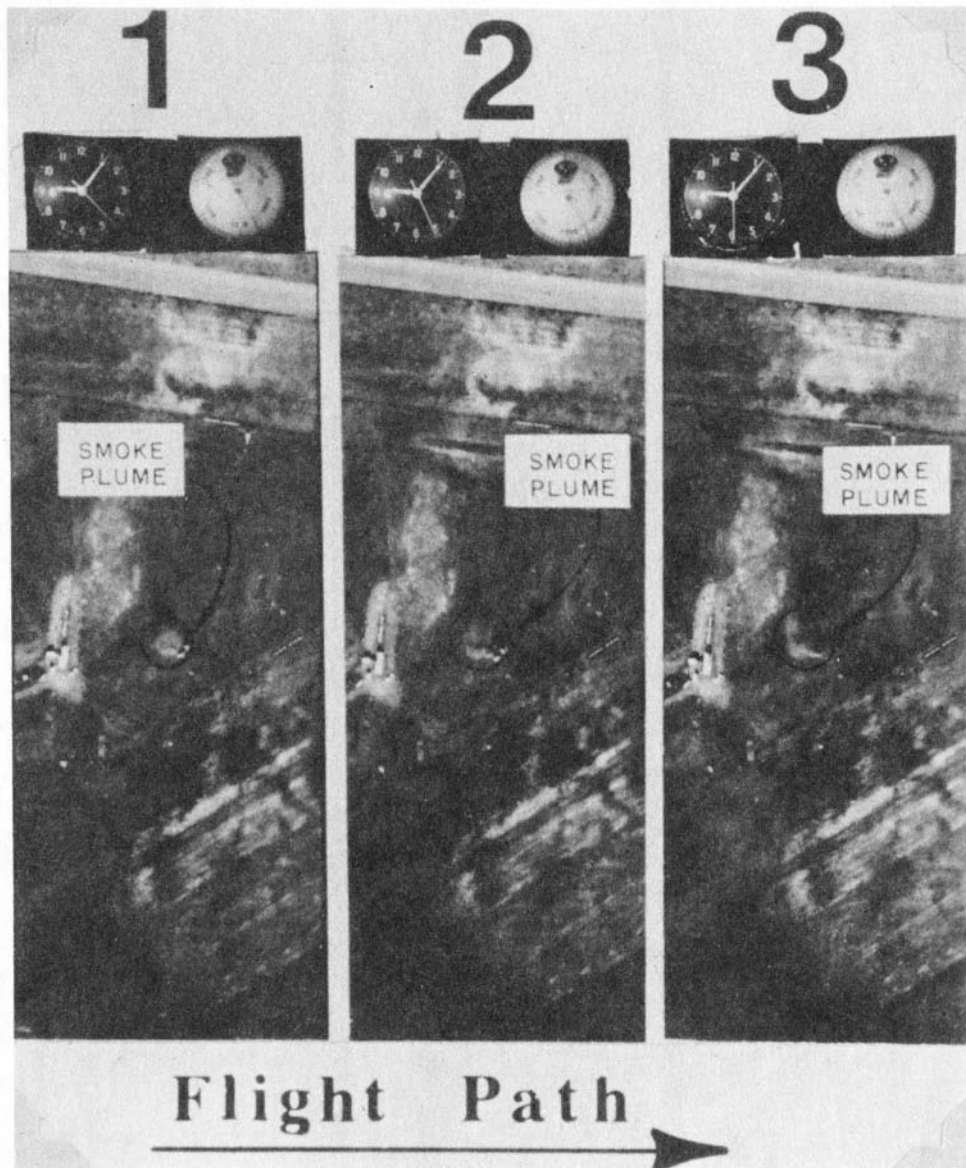


Fig. 5 Reproduction of colored stereo-image triplets of smoke circulation taken from an altitude of 2000 ft.

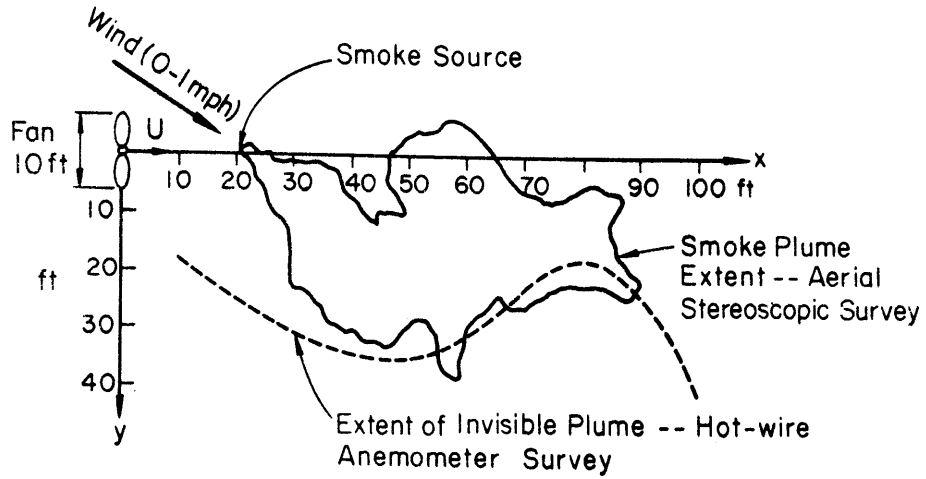


Fig. 6 Planar extent of visible smoke plume and its corresponding invisible plume.